Electron dynamics in α-quartz induced by two-color 10-femtosecond laser pulses

Guillaume Duchateau,[1,*,†] Atsushi Yamada,[2,*,‡] and Kazuhiro Yabana[2]
[1]*CEA, CESTA, 15 Avenue des Sablières, CS60001, 33116 Le Barp Cedex, France*
[2]*Center for Computational Sciences, University of Tsukuba, 1-1-1 Tennodai, Tsukuba, Ibaraki 305-8577, Japan*

(Received 28 May 2021; revised 31 March 2022; accepted 5 April 2022; published 15 April 2022)

The time dependent density functional theory (TDDFT) is used to study the femtosecond laser induced excitation dynamics of electrons in bulk α-quartz, and evaluate the laser energy deposition into this material. In order to properly distinguish the contributions of ionization (electron transitions from the valence band to the conduction band) and laser heating (electron transitions in the conduction band), two 10-femtosecond laser pulses exhibiting different wavelengths are used. Short wavelengths are expected to enhance the ionization rate, whereas longer wavelengths should be more suitable for excitation in the conduction band, thus providing a possible control of the whole electron dynamics. The influence of the pulse-to-pulse delay and intensities is studied. A significant enhancement of the interaction efficiency, in terms of excited electron density and their energy density, is observed for zero pulse-to-pulse delay. It is attributed to the opening of new ionization pathways involving various combinations of both photon energies ensuring the energy conservation, i.e., the sum of photon energies bridges the bandgap. This analysis is supported by a semi-analytical quantum model in the multiphoton absorption regime. The role and strength of direct interband transitions for the electron dynamics in the conduction band are highlighted. The associated laser energy deposition into the material is shown to be as efficient as collisional processes.

DOI: 10.1103/PhysRevB.105.165128

I. INTRODUCTION

The interaction of femtosecond laser pulses with dielectric materials is theoretically studied since the development of such laser facilities, see for example [1–3]. The interest of such works is twofold. First, on the fundamental point of view, this physical system exhibits a complex dynamics due to various mechanisms including electron excitation and relaxation. Despite the main laser induced electron dynamics is now relatively well theoretically described, some points remain to be elucidated as the relative role of intra- and interband electron transitions, and the influence of the real band structure more generally. Advances have been made recently but modeling still include assumptions on the band structure [4–10]. Second, the theoretical study of the interaction of femtosecond pulses with dielectric material is of interest for application purposes including local modification of the refractive index, material structuring, or surface ablation [11–16]. A deep understanding of the processes at play allows one to clearly interpret experimental observations and ultimately allows one to design future experiments and may pave the way to new applications. Such material modifications are generally due to the laser energy deposition into the material, which results from the primary stage of laser induced electron dynamics [14]. Theoretical advances on the interaction of femtosecond laser pulses with dielectric materials are thus still desirable.

The phenomenology of the femtosecond laser induced electron dynamics in dielectric materials is as follows. The first excitation step consists of electron transition from the valence band to the bottom of the conduction band through multiphoton absorption or tunneling [17]. This is the so called photoionization process. The promoted electrons may then further absorb photons in the conduction band, i.e., make conduction-conduction transitions; it is the so-called laser heating. This process may be assisted by a third particle to satisfy both energy and momentum conservations, i.e., photon absorption takes place during the collision with a phonon, an ion, or another electron [18]. In that case intraband transitions mainly take place. The photon absorption may also lead to interband transitions where the lattice ensures the momentum conservation [8,9,19–21]. Collisional processes also take place without involving a photon absorption. They lead to a relaxation of the conduction electrons in the sense their distribution tends towards a Fermi-Dirac distribution, and they have transferred some energy to the lattice. Depending on laser parameters, conduction electrons may reach an energy of the order of the bandgap, leading to impact ionization: the collision of a high-energy conduction electron with a valence electron lead to two electrons in the bottom of the conduction band. The last relaxation process consists of the recombination of excited electrons to the valence band or defective states. The timescale for significant relaxation processes is in excess of $\sim$100 fs [9,18], i.e., they are not significant on an ultrashort timescale corresponding to few-cycle laser pulses ($\sim$10 fs).

Most of theoretical and numerical approaches to describe the previous laser induced electron dynamics, within the

*These authors contributed equally to this paper and are joint first authors.
†Corresponding author: guillaume.duchateau@cea.fr
‡Corresponding author: ayamada@ccs.tsukuba.ac.jp

framework of above mentioned applications, consider the collisional/relaxation processes associated with long enough laser pulses. For instance, a simple and computationally efficient approach is based on rate equations, which only consider the temporal evolution of a few electron populations [22]. A more elaborated description relies on the resolution of Bloch equations [23–28]. Despite such approaches have been shown to provide insights on the electron dynamics, they do not account properly for the material band structure (for instance the assumption of parabolic bands is often used). The laser-induced dynamics in the conduction band thus is only partially described, and not correctly describes the interband transitions (transition between two states in the conduction band). First-principles calculations as the time dependent density functional theory (TDDFT) is able to predict accurately the full band structure and account properly for the interband transitions [29–37]. Such approaches describe all processes including photoionization and laser electron heating in the conduction band (except collisions for standard *ab initio* calculations, see below). However due to this completeness, the evaluation of the contribution of each process to the overall electron dynamics and subsequent energy deposition into the material is not straightforward. Such a distinction could be carried out by shaping the laser pulse or using a complementary theoretical approach.

The present paper aims at investigating in detail by using the TDDFT approach such excitation processes including in particular the direct interband valence-conduction and conduction-conduction transitions. For that purpose, two ultrashort (∼10 fs) laser pulses with different colors are used. Such a color shaping have been shown to be efficient to control the contribution of different processes to the whole electron dynamics in case of relatively long pulses [38–43]. For instance the shorter the wavelength, the larger the photoionization rate, and the lesser efficient the laser heating of conduction electrons. In particular, by providing a realistic description of the material band structure, a further goal of the present paper is to study whether the conclusions on the importance of direct interband transitions for the laser energy deposition stand (previous approaches assumed simplified band structures including the parabolic band approximation [5,9,19–21]). The use of two-color pulses is also of interest for application purposes. It has been shown experimentally and theoretically that changing the delay between relatively long pulses allows one to control the energy deposition into the material (i.e., the electron dynamics), with a possible maximum energy deposition for a nonzero delay [39,44,45].

Section II presents briefly the TDDFT approach used in the present paper. In order to distinguish the contribution of various interband transitions to the electron dynamics and study conditions optimizing the laser energy absorption with ultrashort laser pulses, simulations are conducted by varying both the pulse-to-pulse delay and pulse intensities. The obtained results are shown in Sec. III. For various laser intensities, both the produced electron density in the conduction band and their energy density as a function of the pulse-to-pulse delay are calculated, showing their enhancement in the shortest delay region. The energy distribution of electrons is also evaluated with various laser parameters, providing an in-depth understanding of the electron dynamics. In particular, the influence of the band structure on the energy distribution of laser induced conduction electrons and their absorption is evidenced, together with the role of the pulse color on the electron dynamics. Finally the contribution of interband transitions compared with collisional absorption is evaluated. Main conclusions of this paper are drawn in Sec. IV. In order to support analysis of TDDFT results regarding the photoionization, the so-called BVkP semi-analytical model is used [46,47]. Such an approach has been shown to be able to capture the main trends of the ionization process. The main ingredients of the BVkP approach and some results are presented in Appendix for the sake of clarity, together with an analytical demonstration devoted to the two-color interaction.

II. THEORETICAL DESCRIPTION OF LASER PULSES INTERACTION WITH ELECTRONS IN DIELECTRIC SOLIDS

This section aims at presenting briefly the theoretical model used in the present paper, references are provided for further details. For all calculations, a linearly-polarized two-color laser electric field is used. A fundamental laser pulse and its second harmonics are considered. The amplitude of the total laser electric field reads:

$$E(t) = E_1 \cos(\omega t) f(t) + E_2 \cos\left(2\omega(t-\Delta t)\right) f(t-\Delta t), \tag{1}$$

where the field envelope $f(t)$ is defined as

$$\begin{aligned} f(t) &= \sin^4(\pi t/\tau) \quad \text{if } 0 < t < \tau \\ &= 0 \qquad\qquad\quad \text{otherwise.} \end{aligned}$$

E_1 and E_2 are the electric field amplitudes of the fundamental pulse and it second harmonics, respectively, which are related to the intensity I_i as $E_i = \sqrt{8\pi I_i/c}$ where $i = 1, 2$, and c is the speed of light. In the present paper, we choose $\hbar\omega = 1.55$ eV ($2\hbar\omega = 3.1$ eV) for the fundamental pulse (second harmonics), which corresponds to the widely-used femtosecond Titanium:Sapphire laser facility. The pulse duration is set to $\tau = 26$ fs, which roughly corresponds to 10 fs FWHM. The pulse-to-pulse delay Δt is positive when the fundamental laser pulse first irradiates the target.

To describe electron dynamics induced by a laser pulse, the first-principles calculation based on TDDFT is carried out by using our developed open source software, SALMON [34]. The computational method is briefly explained in this section. Full explanations were given in previous publications [48–50].

The real-space electron orbitals $\{\psi_i(\vec{r}, t)\}$ in a periodic crystalline solid can be expressed based on the Bloch theorem by introducing the reciprocal k space,

$$\psi_i(\vec{r}, t) = e^{i\vec{k}\cdot\vec{r}} u_{b\vec{k}}(\vec{r}, t), \tag{2}$$

where $u_{b\vec{k}}$ is the bth Bloch orbital in a unit cell at the $\vec{k}$ point. To calculate the time-evolution of the orbitals in the external electric field, the time-dependent Kohn-Sham (TDKS)

equation [51],

$$i\hbar\frac{\partial}{\partial t}u_{b\vec{k}}(\vec{r},t)=\left[\frac{1}{2m_e}\left\{-i\hbar\nabla+\hbar\vec{k}+\frac{e}{c}\vec{A}(t)\right\}^2+v_H(\vec{r},t)\right.$$
$$\left.+v_{xc}(\vec{r},t)+\hat{v}_{\rm ion}\right]u_{b\vec{k}}(\vec{r},t), \quad (3)$$

is solved using real-space and real-time method [52]. The four terms of the Kohn-Sham Hamiltonian in the right-hand side represent the kinetic energy operator with electron mass m_e, Hartree potential v_H, exchange-correlation potential v_{xc}, and ionic potential $v_{\rm ion}$, respectively. The kinetic energy operator includes k-vector term $\hbar\vec{k}$ due to the Bloch theorem and vector potential term $\frac{e}{c}\vec{A}(t)$ in this gauge, where $\hbar$, e, and c are Planck constant, the speed of light and the electron charge, respectively.

Our analyses in the next section are based on the excitation energy $E_{\rm ex}$ and the number of excited (conduction) electrons $n_{\rm ex}$ at the end of the interaction. $E_{\rm ex}$ is defined as the difference of the total energy density relative to the ground state. In general, this can be evaluated directly from the total energy calculations. We however calculate it from the field work since the TBmBJ exchange-correlation potential that is not derived from energy density is employed in this paper, that is,

$$E_{\rm ex}(t)=\int^t\vec{E}(t')\cdot\vec{J}(t')dt', \quad (4)$$

where $\vec{E}(t)=-\frac{1}{c}\frac{d}{dt}\vec{A}(t)$ and $\vec{J}(t)$ are the laser electric field and the electric current density, respectively. $\vec{J}(t)$ is defined from the probability flow of electrons integrated over the unit-cell volume [33,51,53,54].

$n_{\rm ex}$ defined in the unit cell is evaluated by:

$$n_{\rm ex}=n_{\rm tot}-\frac{1}{\Omega}\sum_{bb'\vec{k}}f_{b'\vec{k}}\left|\langle u^0_{b\vec{k}}|u_{b'\vec{k}}(t_e)\rangle\right|^2, \quad (5)$$

where $n_{\rm tot}$ denotes the total number of electrons in the unit cell, Ω the unit-cell volume, and $u^0_{b\vec{k}}$ and $f_{b\vec{k}}$ are the Bloch orbital function and its occupation number in the ground state. t_e stands for the time when the laser pulses end. The occupation number distribution as a function of energy is calculated by

$$\frac{dn}{d\epsilon}=\sum_{bb'\vec{k}}f_{b'\vec{k}}\delta\left(\epsilon-\epsilon^0_{b\vec{k}}\right)\left|\langle u^0_{b\vec{k}}|u_{b'\vec{k}}(t_e)\rangle\right|^2, \quad (6)$$

where $\epsilon^0_{b\vec{k}}$ is the orbital energy in the ground state.

The plots of $n_{\rm ex}$ and $E_{\rm ex}$ in the next section are given by dividing by the number of atom per cell, then are in units of atom^{-1} and eV/atom, respectively.

Computational details of the TDDFT calculations are as follows. The cuboid unit cell of SiO_2 with the side length of 4.913 Å, 8.510 Å, and 5.405 Å contains 18 atoms [55]. Uniform spatial grid points of $20\times28\times28$ are set in the cell and 4^3 k points are used in the reciprocal space. This discretization is sufficient to obtain converged results [56,57]. Norm-conserving pseudopotential is employed for the ionic potential. In the present analysis, it is important to use a functional that reproduces accurately the bandgap. We use the TBmBJ functional at the meta-GGA level for the exchange-correlation potential that is known to reproduce bandgaps of insulators systematically [58]. With a value of 1.0 for the TBmBJ parameter, the calculated bandgap energy is 7.7 eV and the first absorption peak obtained from the transition moment analysis is at 9.05 eV, which are in a good agreement with the experimental observations, including the optical response through the dielectric function ([33,59] and references therein). The TDKS equation is integrated with a time step of 0.48 as.

Since we use perfect crystalline structure with frozen atomic coordinates corresponding to a lattice at 0 K, phonon-assisted intraband and indirect interband transitions are not described; only direct (vertical) interband transitions are reproduced. The electron-electron collision is also not properly taken into account in our calculation due to the adiabatic approximation of the used exchange-correlation functional. Since the interaction with 10-femtosecond laser pulses is considered in the present paper, collisional processes are not expected to provide a significant contribution to the whole electron dynamics, neither the electron recombination, which significantly contributes to the whole electron dynamics on a longer timescale [12].

III. RESULTS AND DISCUSSION

A. Study of electron populations

1. Total excited electron density

Figure 1 shows the evolution of the number of excited electrons per atom as a function of the pulse-to-pulse delay, as predicted by TDDFT calculations. Various couples of laser intensities are considered in order to explore different regimes of interaction: (a) $I_1=4.86\times10^{12}$ W/cm^2 and $I_2=10^{12}$ W/cm^2; (b) $I_1=1.95\times10^{13}$ W/cm^2 and $I_2=10^{13}$ W/cm^2; (c) $I_1=1.26\times10^{14}$ W/cm^2 and $I_2=10^{14}$ W/cm^2; (d) $I_1=10^{14}$ W/cm^2 and $I_2=10^{13}$ W/cm^2. Cases (a), (b), and (c) corresponds to a configuration where each single-color pulse produces a similar number of excited electrons as the other color (a single-color pulse electron production is evaluated by switching off the other pulse). Going from cases (a) to (c), the intensity is increased, inducing electron production through multiphoton absorption and tunneling, respectively. In case (d), the number of excited electrons produced by each single-color pulse are different. These electron numbers for each configuration are summarized in Table I.

For all configurations as shown in Fig. 1, the evolution of the number of excited electrons with respect to the pulse-to-pulse delay exhibits a similar shape: it is symmetric with respect to the zero delay and, the longer the delay, the smaller the electron excitation. In the region of short delays, i.e., shorter than ~5 fs, there are oscillations with a period of ~0.66 fs.

The main shape can be explained following results provided in the literature for longer pulses [39,43]. For the longest delays where pulses do not overlap, each pulse produces independently excited electrons. In the multiphoton regime, excited electrons are produced through simultaneous absorption of 6 photons and 3 photons by ω pulse and

TABLE I. Excited electron densities (in units of atom^{-1}) with various laser parameters as predicted by TDDFT calculations. $n_{ex}^{(1)}$ and $n_{ex}^{(2)}$ correspond to the excited electron densities by a single laser pulse with frequency ω and 2ω, respectively.

	$n_{ex}^{(1)}$	$n_{ex}^{(2)}$	$n_{ex}(\Delta t=0)$	$n_{ex}(\Delta t=0)/(n_{ex}^{(1)}+n_{ex}^{(2)})$
(a) $I_1 = 4.86\times10^{12}$ W/cm^2 and $I_2 = 10^{12}$ W/cm^2	2.191×10^{-7}	2.220×10^{-7}	1.307×10^{-5}	29.7
(b) $I_1 = 1.95\times10^{13}$ W/cm^2 and $I_2 = 10^{13}$ W/cm^2	1.588×10^{-4}	1.625×10^{-4}	4.582×10^{-3}	14.3
(c) $I_1 = 1.26\times10^{14}$ W/cm^2 and $I_2 = 10^{14}$ W/cm^2	7.978×10^{-2}	7.983×10^{-2}	3.736×10^{-1}	2.3
(d) $I_1 = 10^{14}$ W/cm^2 and $I_2 = 10^{13}$ W/cm^2	4.704×10^{-2}	1.625×10^{-4}	7.722×10^{-2}	1.6

2ω pulse, respectively. The higher the intensity, the larger the electron production, see Table I. In that case, the total produced electron number is the sum of each single-pulse contribution: $n_{ex}(\Delta t=\pm\tau) = n_{ex}^{(1)} + n_{ex}^{(2)}$ (the decrease of valence occupation induced by the first pulse is not significant so that it does not affect the second-pulse excitation). For shorter delays where pulses overlap, the total laser intensity gets higher, and additional quantum excitation pathways appear. For instance the bandgap can be bridged through the simultaneous absorption of 2 photons at 3.1 eV and 2 photons at 1.55 eV, or 1 photon at 3.1 eV and 4 photons at 1.55 eV. The total excitation probability increases with respect to the number of excitation pathways, explaining the curve rise when the delay decreases. The latter influence is the most important for a zero delay where pulses fully overlap, leading to the highest total laser intensity and largest probabilities for each photon combination. This situation thus corresponds to the largest enhancement in the production of excited electrons. The higher the intensities, the smaller the enhancement defined as $n_{ex}(\Delta t=0)/(n_{ex}^{(1)}+n_{ex}^{(2)})$ (see Table I). Indeed going to the tunneling regime, i.e., departing from the multiphoton absorption regime, the ionization process less depends on the photon energy. The above mentioned combinational effect of photon absorption is thus less important. In addition, in this regime, the excitation probability less varies with respect to intensity compared to the perturbative multiphoton regime. It thus turns out that low intensities is the most favorable configuration to enhance electron production by pulses overlapping. In perturbative conditions, since the population of the valence band remains almost unchanged after the interaction with one pulse, all previous processes little depend on the delay sign leading to almost symmetric curves with respect to the delay as observed in Fig. 1. Asymmetry is observed for the deposited energy as shown later.

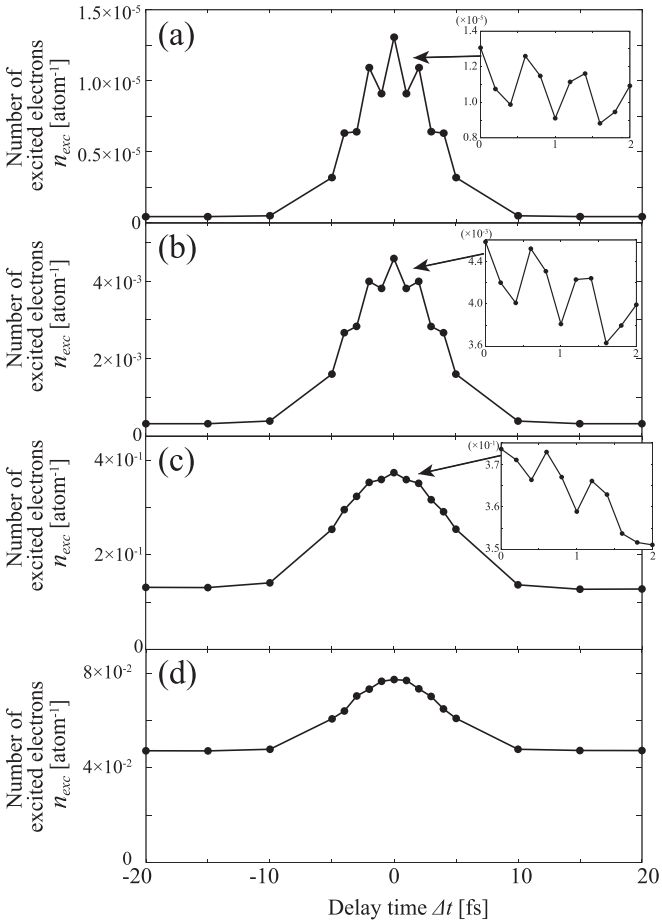

FIG. 1. Number of excited electrons per atom as a function of the pulse-to-pulse delay obtained by TDDFT calculations. Various couples of laser intensities are used: (a) $I_1 = 4.86\times10^{12}$ W/cm^2 and $I_2 = 10^{12}$ W/cm^2; (b) $I_1 = 1.95\times10^{13}$ W/cm^2 and $I_2 = 10^{13}$ W/cm^2; (c) $I_1 = 1.26\times10^{14}$ W/cm^2 and $I_2 = 10^{14}$ W/cm^2; (d) $I_1 = 10^{14}$ W/cm^2 and $I_2 = 10^{13}$ W/cm^2. Insets of (a), (b), and (c) show a zoom in the short delay region with more data points to better exhibit the oscillation-like behavior (see text).

Regarding the observed oscillations in the region of short delays, the local maxima of the excited electron number take place at delays of 0, 0.66 fs, 1.33 fs, 2.0 fs, etc., and the local minima at 0.33 fs, 1.0 fs, 1.66 fs, etc. The period of oscillations of 0.66 fs corresponds to a frequency 4ω where both electric fields are in phase so that the total field amplitude is modulated. This behavior was also observed for atomic target without delay but varying the pulse-to-pulse relative phase [60] (which is similar to our conditions for not too large delays). As shown in Appendix, the same oscillation-like behavior is retrieved with the BVkP approach with similar laser parameters. The BVkP approach being computationally efficient, simulations with various couples of laser intensity have been performed (results not shown). The period of 0.66 fs is always obtained, thus indicating this is a general feature of the present interaction. To illustrate the origin of maxima and minima in the excited electron number, the temporal evolution of the total laser electric field is shown in Fig. 2 for delays of (a) $\Delta t = 0$ and (b) $\Delta t = 0.33$ fs, which are representative of above-mentioned other delays. The laser intensities are those of Fig. 1(a). Note that despite fields are asymmetric with respect to the horizontal axis, the vector potential is always zero at the end of the interaction for all delays. Maxima and minima in the excited electron number can be attributed to the fact that the maximum total field is different depending

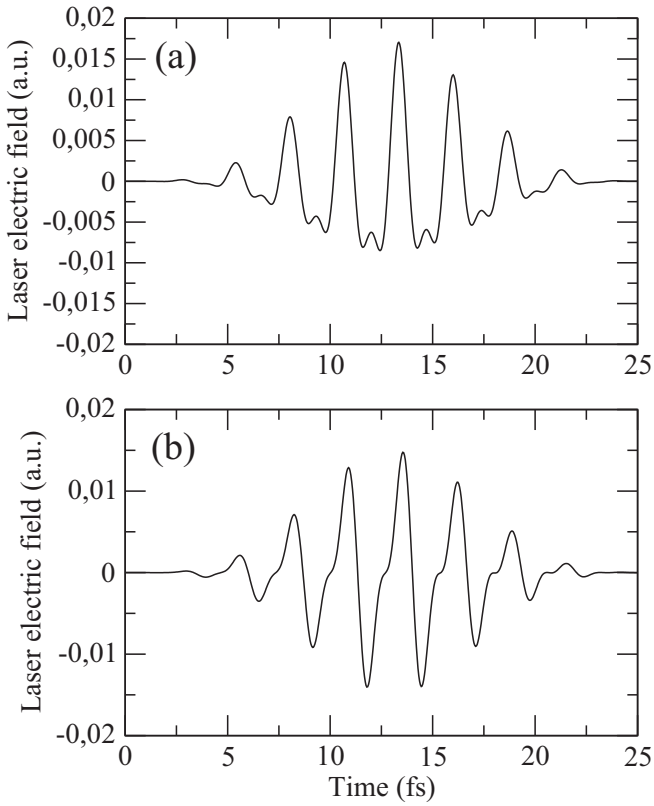

FIG. 2. Temporal evolution of the total laser electric field for two pulse-to-pulse delays: (a) $\Delta t = 0$; (b) $\Delta t = 0.33$ fs.

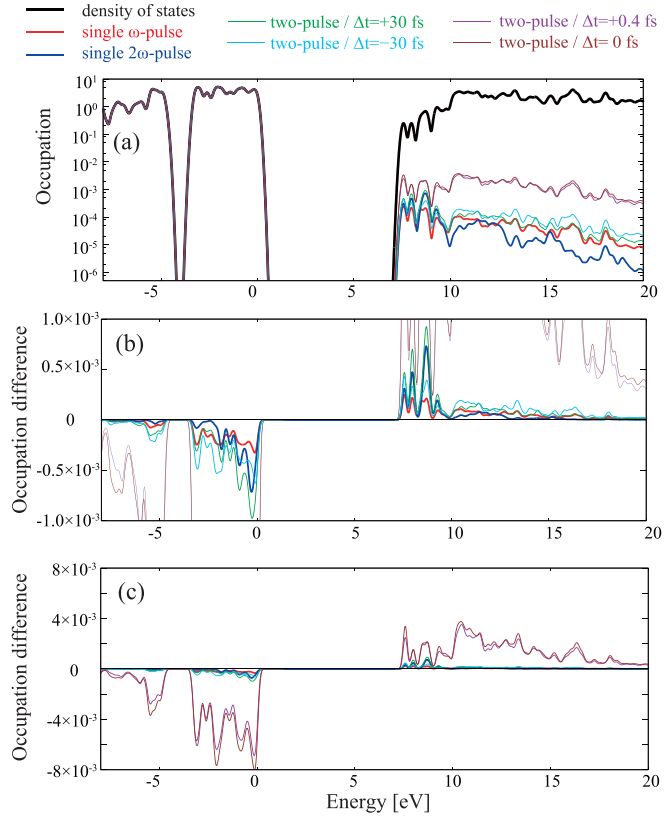

FIG. 3. Band occupation with respect to the electron energy as predicted by TDDFT calculations. Results with single pulses and two pulses with various delays are shown (see legend at top). The chosen intensities are $I_1 = 1.95 \times 10^{13}$ W/cm^2 and $I_2 = 10^{13}$ W/cm^2.

on the delay. Since the electron excitation takes place through nonlinear interaction, the larger maximum field amplitude for $\Delta t = 0, 0.66$ fs, 1.33 fs, ... explains the observed local maxima in the electron number. Note that the higher the laser intensities, the smaller the amplitude of these oscillations as shown by Fig. 1. This behavior may be explained by the fact that going to the tunneling regime, the excitation probability is less sensitive to the electric field amplitude. The analysis of previous TDDFT results is supported by numerical calculations with the BVkP approach as shown in Appendix.

Overall previous results clearly show that the higher the laser intensities, the smaller the enhancement ratio, which may be explained by two main reasons: (i) the enhanced excitation based on combinational two-color photon absorption requires a full perturbative regime, thus lowest intensities as possible. The larger the intensity, the more significant excitation though tunnel effect, the less efficient the combinational patterns. (ii) For large laser intensities, a single pulse by itself may significantly empty the valence band, the second pulse thus can no longer excite removed valence electrons, reducing the two-pulse cooperation.

2. Band occupation

In order to get a better picture of the laser induced full electron dynamics including transitions in the conduction band, the band occupation with respect to the electron energy as predicted by TDDFT calculations is plotted in Fig. 3 for various laser configurations: single pulses and two pulses with various delays. The chosen intensities are $I_1 = 1.95 \times 10^{13}$ W/cm^2 and $I_2 = 10^{13}$ W/cm^2, corresponding to results of Fig. 1(b). We remind that the number of excited electrons induced by each single pulse is the same.

The results of single-pulse irradiation are first considered. Fig. 3(a) shows that the occupation of excited electrons (in the conduction band) mainly mimics the DOS (density of states) by reproducing the sub-structures (succession of bumps and deep parts) as expected. However depending on the photon energy, the energy distribution of excited electrons is different: the occupation induced by the 2ω pulse below $\sim$10 eV is larger than the ω pulse one, and the opposite behavior is observed above 10 eV. These energy distributions can first be explained by the fact that, at $2\omega = 3.1$ eV, the peaks in the population at $8 - 9$ eV can only be due to three-photon absorption (two-photon absorption is forbidden) whereas the population induced in this region at $\omega = 1.55$ eV is due to five-, six-, and seven-photon absorption. The latter process explains the spreading of excited electrons distribution and thus smaller peaks (number of excited electrons induced by each color is the same). The second influence explaining this discrepancy is the further photon absorption by primary excited electrons at the threshold of the conduction band (electron transitions in the conduction band, or laser heating of conduction electrons). We have checked that the amplitude of the transition moment is larger at 1.55 eV by a factor of $\sim$3 compared with 3.1 eV. It follows that the excited electrons to the

bottom of the conduction band can be further excited to higher energies (through interband transitions) more efficiently with 1.55 eV photons than with 3.1 eV, further explaining the lower ω population below 10 eV, and the higher for larger energies with a non-negligible population up to ∼18 eV. The latter observation is better supported by Fig. 3(b), which shows the change in occupation distribution from the unperturbed ground state within a linear scale. Note that $I_1 > I_2$ further enhances the electron heating process.

Now the two-pulse case without overlap is considered (delays of ±30 fs). The comparison with the previous results of single-pulse interaction is first carried out. Compared with the single-pulse irradiation at 1.55 eV, the irradiation of the material by the ω pulse followed by the 2ω pulse at $\Delta t = +30$ fs leads to a strong increase in the electron population below 10 eV. An increase above 10 eV also takes place but clearly in a lesser extent. The previously discussed electron dynamics induced by the 2ω pulse is thus retrieved: this frequency bridges the valence band to the conduction band more efficiently than states in the conduction bands (conduction-conduction transitions). Compared with the single-pulse irradiation at 3.1 eV, the following ω pulse leads to the opposite behavior: the electron population below 10 eV is decreased whereas the population above is strongly increased. This dynamics is consistent with previous considerations indicating that the ω pulse is strongly efficient to heat conduction electrons, thus depopulating 2ω-induced electrons below 10 eV. It thus turns out that the irradiation chronology by two pulses of different colors influences the electron dynamics. Within the present conditions where each single pulse produces the same number of excited electrons, the configuration where the shorter wavelength pulse first irradiates the material leads to the larger total electron energy, and subsequent laser energy deposition into the material.

To conclude this section, the configuration of two pulse with a strong overlap is considered. Figure 3(c) shows the change in occupation distribution from the unperturbed ground state for delays of 0 and 0.33 fs. We remind that the zero delay corresponds to the production of the largest number of excited electrons, and a delay of 0.33 fs to the first local minimum in this number. This observation is retrieved here since the average occupation is significantly larger with the pulse overlap. The interesting resulting feature of this overlapped configuration is that the shape of the electron energy distribution is strongly affected compared with the previous case without overlap. Contrary to the previous distribution where the highest occupations are in the range $0 - 10$ eV, here they are located slightly above 10 eV. If the peak at the threshold is excluded, higher occupations even take place up to roughly 17 eV. The laser heating efficiency is thus enhanced through the simultaneous cooperation of both colors. We suggest it is due to new possibilities to satisfy resonant condition (interband transition in the conduction band) through the possible sequential or simultaneous absorption of several photons involving both colors. In particular the probability for these new allowed transitions become larger owing to various combinations of both photon energies as for the excitation from the valence to the conduction band. Note that as shown in the next section, the enhancement ratio in the total energy

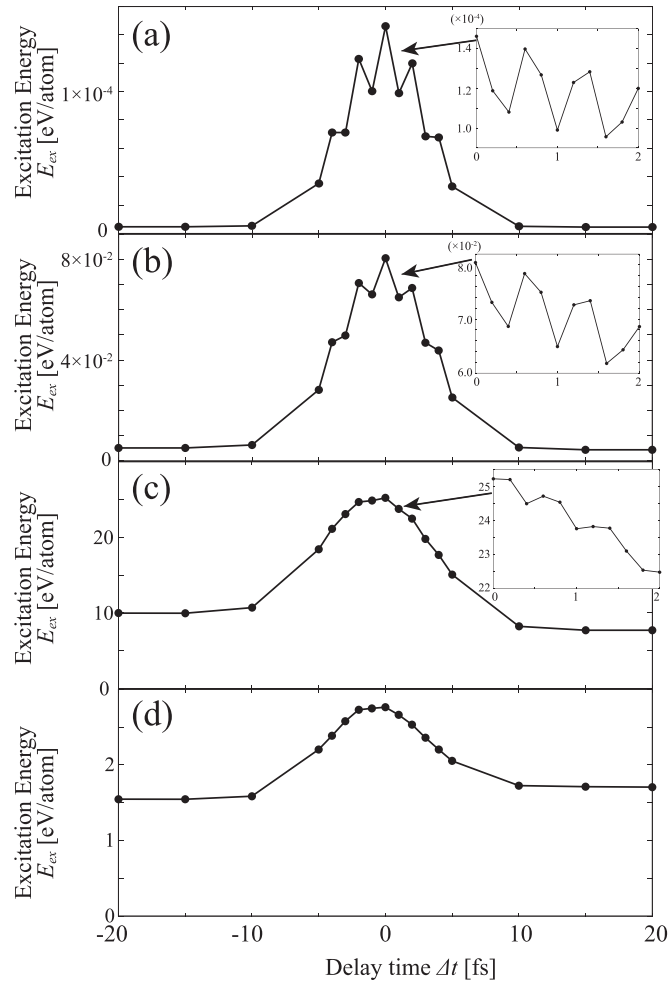

FIG. 4. Energy of excited electrons per atom as a function of the delay between pulses as obtained with TDDFT calculations. Various laser intensities are used: (a) $I_1 = 4.86 \times 10^{12}$ W/cm^2 and $I_2 = 10^{12}$ W/cm^2; (b) $I_1 = 1.95 \times 10^{13}$ W/cm^2 and $I_2 = 10^{13}$ W/cm^2; (c) $I_1 = 1.26 \times 10^{14}$ W/cm^2 and $I_2 = 10^{14}$ W/cm^2; (d) $I_1 = 10^{14}$ W/cm^2 and $I_2 = 10^{13}$ W/cm^2. Insets of (a), (b), and (c) show a zoom in the short delay region with more data points to better exhibit the oscillation-like behavior (see text).

of excited electrons is of the same order as the one for the number of excited electrons per atom, thus suggesting the main contribution to the total electron energy density remains the number of excited electrons.

B. Study of electron energy density

This section is devoted to study the laser energy deposition into the material, i.e., the excited electron energy density. Preliminary trends have been obtained by studying the energy distribution of excited electrons. The ω pulse is more efficient to heat primary produced conduction electrons, and subsequently the two-pulse configuration where the 2ω pulse first irradiates ($\Delta t < 0$) leads to the highest energetic electrons.

Figure 4 shows the energy per atom of excited electrons as a function of the pulse-to-pulse delay for same couples of intensities as in Fig. 1. The main shapes are relatively similar to those of excited electron density, the longer the delay, the

TABLE II. Excited electron energy per atom with various laser parameters. $E_{ex}^{(1)}$ and $E_{ex}^{(2)}$ correspond to the excited electron energy densities by a single laser pulse with frequency ω and 2ω, respectively.

	$E_{ex}^{(1)}$	$E_{ex}^{(2)}$	$E_{ex}(\Delta t = -30$ fs)	$E_{ex}(\Delta t = +30$ fs)
(a) $I_1 = 4.86 \times 10^{12}$ W/cm^2 and $I_2 = 10^{12}$ W/cm^2	2.267×10^{-6}	2.112×10^{-6}	4.660×10^{-6}	4.453×10^{-6}
(b) $I_1 = 1.95 \times 10^{13}$ W/cm^2 and $I_2 = 10^{13}$ W/cm^2	2.254×10^{-3}	1.765×10^{-3}	5.168×10^{-3}	4.421×10^{-3}
(c) $I_1 = 1.26 \times 10^{14}$ W/cm^2 and $I_2 = 10^{14}$ W/cm^2	3.141	2.427	10.0	7.720
(d) $I_1 = 10^{14}$ W/cm^2 and $I_2 = 10^{13}$ W/cm^2	1.540	1.765×10^{-3}	1.546	1.709

smaller the electron energy. The oscillation-like behavior is also observed, with the same period of ∼0.66 fs. However, the curves are no longer symmetric with respect to the zero delay. The higher the intensities, the more asymmetric the evolution of the electron energy. A summary of representative data is provided in Table II, including the excitation energy density induced by a single-color pulse.

The fact that the evolution of the excited electron energy exhibits similar trends as the number of excited electrons is due to the ionization process (electron transition from the valence to the conduction band), which contributes significantly to the value of both quantities. Obviously the number of excited electrons is fully due to the ionization process. The latter induces a significant number of electrons in the 10 eV range, which thus makes the total electron energy related to the number of excited electrons. It follows the enhancement in the energy density (between zero delay and ±30 fs delay) is of the same order of magnitude as for the excited electron densities. Actually the value of the excited electron energy is due to two processes: (i) ionization and (ii) heating in the conduction band. The energy density for process (i) is of the order of $E_{vc} \sim n_{ex}E_g \sim 6\hbar\omega n_{ex}$. Since TDDFT calculations provide the total electron energy density E_{ex}, the contribution of process (ii) is $E_{cc} = E_{ex} - E_{vc}$. In order to highlight the electron dynamics in the only conduction band (by not including the contribution of the ionization process), the ratio E_{ex}/n_{ex} can be considered, which corresponds to the average energy of a single excited electron at the end of the interaction. For illustration purpose, this ratio is plotted in Fig. 5 for the intensity couple $I_1 = 1.95 \times 10^{13}$ W/cm^2 and $I_2 = 10^{13}$ W/cm^2. A pure ionization process would have lead to a value of E_{ex}/n_{ex} not evolving with the pulse-to-pulse delay, of the order of the bandgap energy. The observed variations in Fig. 5 are thus the signature of the contribution of conduction-conduction transitions. For this intensity configuration, $E_{ex}/n_{ex}(\Delta t = -30$ fs) ∼ 16 eV and $E_{ex}/n_{ex}(\Delta t = +30$ fs) ∼ 14 eV. Assuming the excitation energy from valence to conduction band is $e_{vc} \sim 6\hbar\omega = 9.3$ eV, the gained energy in the conduction band is $e_{cc} = 16 - 9.3 = 6.7$ eV and $e_{cc} = 14 - 9.3 = 4.7$ eV, respectively. Note that despite the multiphoton order for conduction-conduction transitions is lower than for valence-conduction one (see below), the absorbed energy is smaller because this mechanism takes place only when conduction electrons are produced. The remaining available laser energy is thus smaller than the whole laser pulse, which has produced the conduction electron density. The asymmetry of curves $[e_{cc}(\Delta t = -30$ fs$) > e_{cc}(\Delta t = +30$ fs$)]$ is explained by the fact that the ω pulse excites more efficiently conduction electrons than the 2ω pulse, as discussed at the end of Sec. III A. Regarding the enhancement of E_{ex}/n_{ex} for small delays, as for the valence-conduction excitation process, it is most probably due to the contribution of combinational absorption pathways, thus implying a nonlinear absorption in the conduction band where at least simultaneous absorption of two photons with different color is possible at some points in the Brillouin zone. This scenario is supported by the scaling law of e_{cc} with respect to the intensity in the single-color case. By fitting the curve with a power law, the found exponents are 1.13 and 0.994 for the ω pulse and 2ω pulse, respectively. A standard linear absorption is thus found for the 2ω pulse. However for the ω pulse, an exponent larger than unity indicates that some transitions involving two-photon absorption in the conduction band take place. Finally, all previous results are compared with those obtained with longer pulses where collisional and recombination processes contribute significantly to the electron dynamics. First, the enhancement of laser energy deposition into the material is considered. The previous results show that the maximum energy deposition takes place at a zero pulse-to-pulse delay whereas longer pulses (at least 50 − 100 fs) lead to a delay in between ∼100 fs and a few ps depending on the laser features [38,39,44,45,59,61]. In case of longer pulses, electron relaxation, including various collisional processes and electron recombination, play an important role on the electron dynamics. In brief, first irradiation by the short wavelength pulse lead to a significant free electron production, and subsequent irradiation by an infrared laser pulse induces a significant heating

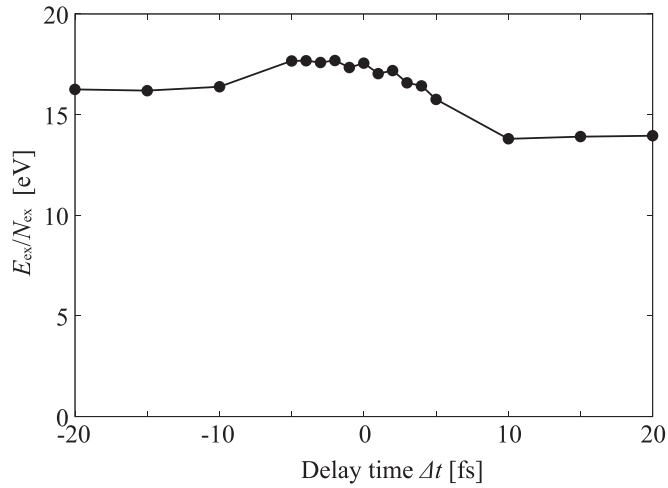

FIG. 5. Ratio of energy of excited electrons over their density as a function of the delay between pulses. Laser intensities are $I_1 = 1.95 \times 10^{13}$ W/cm^2 and $I_2 = 10^{13}$ W/cm^2.

of previously promoted free electrons. If the pulse-to-pulse delay is too short, the population of free electrons is not large enough for a significant absorption of the infrared pulse. If the delay is too long, free electrons produced by the first pulse have significantly recombined, which again lead to a small absorption of the infrared pulse. Therefore there is an optimal delay where the free electron populations produced by the first pulse is the largest and most prompted to be heated by the subsequent infrared pulse to lead to a final significant laser energy deposition. Impact ionization (collision of a conduction electron with a valence electron leading to two conduction electrons) also plays an important role on the delay value since it modifies the free electron population and depends on the subsequent infrared laser heating (this process takes place if the energy of conduction electrons is at least of the order of $3E_g/2$ [22]). In the present paper with ultrashort laser pulses where such relaxation and recombination processes are less important, the direct interband electron transitions drive the whole electron dynamics. It turns out that enhancement of laser energy deposition is due to the increased coupling between states through additional combinations of both photon energies, which thus takes place when both laser intensities are the highest, i.e., at zero pulse-to-pulse delay. However note that in case of nonzero delay, as for longer pulses, this is the configuration of first irradiation by the shorter wavelength pulse, which leads to the larger energy deposition.

The longer wavelength pulse is the most efficient to heat free electrons, whatever the pulse length. However, due to the band structure, the present results for a single ω pulse show that the scaling of the energy deposition (for a given free electron density) with the laser intensity departs from the linear behavior predicted by the Drude model. Since in general both intra- and interband electron transitions contribute to the electron dynamics in the conduction band [5] and subsequent laser energy deposition into the material, the presently exhibited nonlinear absorption is expected to play a role for long pulses ($\tau > 50$ fs). For instance, this effect is expected to modify predictions of energy absorption by free electrons as predicted by models assuming it results from the independent contribution of each color pulse, i.e., sum of single-color contributions [38]. Finally, despite the present TDDFT does not include properly collisional effects, an *effective* collision frequency ν_{eff} associated with the energy deposition can be estimated in a similar way as done in [62]. According to the Drude model, the variations of energy density, E_{ex}, of a gas of independent free electrons reads [63]:

$$\frac{\partial E_{ex}}{\partial t} = \frac{2en_{ex}\nu_{\text{eff}}}{c\varepsilon_0 m_e\left(\omega^2 + \nu_{\text{eff}}^2\right)} \tag{7}$$

where ε_0 is the vacuum dielectric permittivity and other quantities have been defined previously. Knowing the electron density, the effective collision frequency can be evaluated to retrieve the same absorbed energy as the one predicted by TDDFT calculations. Assuming $\nu_{\text{eff}} \ll \omega$, simple calculations lead to $\nu_{\text{eff}} \sim m_e\omega^2 c\varepsilon_0 E_{ex}/e^2 n_{ex} I\tau$. By using values of electron density and energy of Tables I and II, we obtain an effective collision frequency of the order of 1 fs. The latter value is of the same order of magnitude as standard collision frequency including the electron-phonon collision (theoretically predicted or obtained through a Drude model to fit experimental data). The contribution of interband transitions to the laser induced electron dynamics in the conduction band is thus definitively significant whatever the pulse duration.

IV. CONCLUSION

The electron dynamics in α-quartz induced by femtosecond laser pulses has been theoretically studied. Two pulses with different wavelengths have allowed to well distinguish electron transition from the valence band to the conduction band, and the dynamics in the conduction band. Various behaviors have been highlighted by varying both the pulse-to-pulse delay and intensities.

TDDFT calculations show a possible enhancement in excess of one order of magnitude in the density of excited electrons when both pulses fully overlap. This effect is due to the appearance of new quantum ionization pathways involving both photon energies. By varying the pulse-to-pulse delay around the optimal zero value leads to an oscillating like behavior of the excited electron density, which is attributed to modulations in the total laser electric field. These analysis have been supported by a semi-analytical approach (BVkP) capturing the main ionization processes at play within the present laser parameters. The observed trends are thus a general feature of the present physical system.

Regarding the laser induced electron dynamics in the conduction band, the TDDFT calculations show that the coupling between states is the most efficient for longest wavelengths, suggesting the largest laser energy deposition into the material is obtained by first irradiating with the shortest wavelength pulse. The latter efficiently ionizes the material for a subsequent efficient energy deposition through the absorption of conduction electrons. The present results also show that the nonlinear absorption of the laser pulses by conduction electrons may play a role, in particular by combining the simultaneous absorption of photons with different energies. By using the Drude model, an effective collision frequency associated to the interband absorption has been evaluated. It lies in the femtosecond range, which is comparable with values obtained with longer pulses for which the electron collisions are known to play an important role for the laser absorption (through intraband transitions). The present paper, which includes a realistic band structure, thus also confirms that both intra- and inter-band transitions contribute to the laser energy deposition into dielectric materials. Such conclusions may be considered to interpret experimental observations on femtosecond laser processing of dielectric materials (resulting from the energy deposition), and possibly included for designing accurately future experiments.

ACKNOWLEDGMENTS

This research was supported by JST-CREST under Grant No. JP-MJCR16N5, and by JSPS KAKENHI Grants No. 20H2649 and No. 19K05364. Calculations are carried out at Oakforest-PACS at JCAHPC with support through Multidisciplinary Cooperative Research Program in CCS, University of Tsukuba. Fabrice Catoire is acknowledged for fruitful discussions on the BVkP approach.

APPENDIX: THE BVkP APPROACH

1. Principle

The semi-analytical BVkP approach for describing ionization (through multiphoton absorption) in dielectric materials was developed in [46,47], among others as reviewed in [64] for instance. This is a good candidate to support analysis of TDDFT results since it is based on a time-dependent approach well designed to capture specific properties of the two-color pulse interaction. This kind of approach based on Volkov states was validated against predictions of the time-dependent Schrödinger equation for atomic and solid targets in the multiphoton regime, i.e., laser intensities lower than about 10^{13} W/cm^2 within the present conditions [17,46,60,65,66]. Here are recalled the main ingredients and assumptions of this approach, together with an improvement proposed for the present paper.

The BVkP approach is based on an analytical evaluation of the quantum transition amplitude from the initial unperturbed valence state $\varphi_v(\vec{r},t)$ to the final perturbed conduction state $\Psi_c(\vec{r},t)$. Assuming a single-active electron and the electric dipole approximation within the length gauge, the transition amplitude reads:

$$T_{cv}(t) = -i\int_0^t dt\langle\Psi_c(t)|\vec{r}\cdot\vec{E}(t)|\varphi_v(t)\rangle. \tag{A1}$$

$\Psi_c(\vec{r},t)$ is approximated by a Bloch-Volkov state, which describes an electron in both the laser electric field and the crystalline field [67]. By using the $\vec{k}\cdot\hat{P}$ theory to evaluate the matrix element [68], i.e., electron transitions are assumed to take place in the center of the Brillouin zone, and developing the Volkov phase as powers of the vector potential assuming the latter is not too large, calculations leads to

$$T_{cv}(t) = -\frac{P}{m_e E_g}\int_0^t dt\exp\{iE_g t\}\frac{E(t)}{(1-iA(t)/\alpha)^2} \tag{A2}$$

where E_g is the material bandgap, and α is the only parameter of this approach, which is related to the spatial expansion of the valence wavefunction, set to 1.55 a.u. as in [46]. $P=\sqrt{E_g/2m^*_{vc}}$ is related to the matrix element through the $\vec{k}\cdot\hat{P}$ theory, where m^*_{vc} is the electron effective mass.

In general, the excitation probability associated to the transition of a valence electron to the conduction band at the end of the interaction is given by $P_{ex}=\|T_{cv}(\tau)\|^2$. We have recently observed slight differences in the BVkP predictions in out-of-resonance conditions through the transformation $\vec{E}(t)\rightarrow-\vec{E}(t)$, whereas they should not depend on the field orientation within the present symmetric system. This behavior is due to the fact there is no integration over the Brillouin zone so that both k direction are not included (where k is the wave vector). To fix this behavior, $P_{ex}=(\|T^{(+)}_{cv}(\tau)\|^2+\|T^{(-)}_{cv}(\tau)\|^2)/2$ is now calculated, where $T^{(+)}_{cv}(\tau)$ corresponds to Eq. (A2) and $T^{(-)}_{cv}(\tau)$ to the same expression where $-\vec{A}(t)$ substitutes $\vec{A}(t)$. We have verified this modification still provides correct predictions compared with previously published results including simulations solving optical Bloch equations [46].

To study whether several excited states may play a role on the excitation probability (the highest occupied valence state may bridge to states higher than the lowest unoccupied conduction state, i.e., corresponding to above threshold ionization), additional final states can be included in the BVkP approach. The total excitation probability can be estimated as the sum of each partial probability [46]. Note that a deviation from this sum is possible due to interfering pathways [69]. We emphasize this approach is only used to evaluate whether there is an influence or not of above threshold ionization in the case of excitation by two-color laser fields, to support forthcoming analysis of TDDFT results. Overall, the BVkP approach is used in this paper only to support forthcoming analysis of TDDFT results, because it is expected to account for the main features of the photoionization process.

2. Numerical results

In order to support the analysis of TDDFT results presented in the main text, numerical calculations with the BVkP approach have been carried out. The validity of this approach is further supported by the fact that $A/\alpha<1$ within the present conditions, which is required to involve the multiphoton absorption as the major ionization process [46]. Indeed, in atomic units, $A=E/\omega\simeq 0.3$ for $I=10^{13}$ W/cm^2 and a photon energy of 1.55 eV. So that $A/\alpha\simeq 0.2<1$. Figure 6 shows the evolution of the excitation (ionization) probability as a function of the pulse-to-pulse delay for three configurations of intensity couples. Note that TDDFT and BVkP calculations provide the number of excited electrons and excitation probability, respectively, so that only variations with parameters are considered (which is enough to support previous TDDFT analysis).

Figure 6(a) shows the BVkP predictions in the case of resonant excitation ($E_g=9.3$ eV) with a single conduction state. Intensities in the 10^{13} W/cm^2 range are chosen for this first calculation, comparable to those of Fig. 1(b), and have been chosen so that the excitation probabilities induced by each single pulse are similar. We obtain $I_1=6.5\times10^{13}$ W/cm^2, $I_2=10^{13}$ W/cm^2, and $P_1=P_2=7.\times10^{-4}$ [I_2 has been chosen as in Fig. 1(b), providing a value for the excitation probability, and I_1 was then varied to retrieve the same probability]. The fact that I_1 exhibits a different value from the one obtained with TDDFT calculations may be due to the influence of the band structure including possible electron transitions out of the center of the Brillouin zone, with various amplitudes of dipolar matrix elements, which are not included in the BVkP approach. Behaviors of Figs. 6(a) and 1(b) are in a good agreement. The main shape and oscillating-like behavior are retrieved confirming the above mentioned analysis based on electron transitions between valence and conduction states since only this process is included in the BVkP model (there is no transition between conduction states). An analytical demonstration exhibiting the combination of both photon energies leading to an increased transition amplitude, supporting the previous analysis, is provided below. However, the BVkP model predicts more pronounced oscillation-like structures, in particular they still appear for relatively long delays of $\sim$10 fs. Also the two-pulse excitation probability can be smaller than the sum of independent contribution of each single pulse. This observation is analysed in the following paragraph. The BVkP enhancement factor is $\sim$23, which is also relatively close to

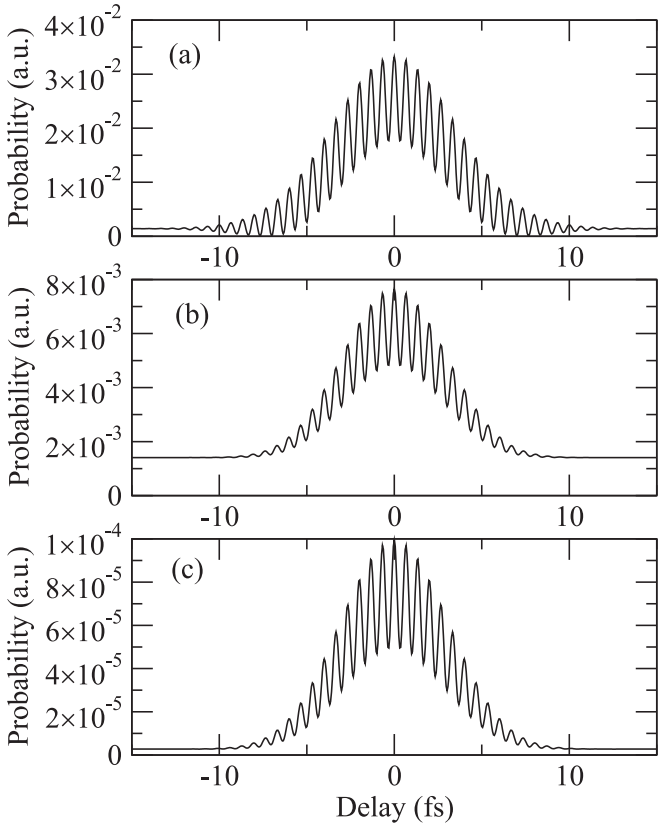

FIG. 6. Evolution of the excitation (ionization) probability as a function of the pulse-to-pulse delay as predicted by the BVkP approach for three configurations: (a) only one conduction state, $E_g = 9.3$ eV, $I_1 = 6.5 \times 10^{13}$ W/cm^2 and $I_2 = 10^{13}$ W/cm^2; (b) 10 conduction levels separated by 0.25 eV, $E_g = 9.05$ eV, $I_1 = 1.95 \times 10^{13}$ W/cm^2 and $I_2 = 10^{13}$ W/cm^2; (c) 10 conduction levels separated by 0.25 eV, $E_g = 9.05$ eV, $I_1 = 1.8 \times 10^{13}$ W/cm^2 and $I_2 = 10^{12}$ W/cm^2.

the TDDFT prediction (14.3). Now the BVkP approach is used within more similar conditions as TDDFT calculations, i.e., $E_g = 9.05$ eV, and the conduction band is described with ten states with an energy difference of 0.25 eV between two adjacent states. The energy of the highest conduction state is thus 2.5 eV (above the bottom of the conduction band), possibly allowing above threshold ionization. Intensities are the same as in Fig. 1(b), thus leading to different excitation probability induced by each single pulse: $P_1 = 2.5 \times 10^{-6}$ and $P_2 = 1.5 \times 10^{-3}$. Figure 6(b) shows the predicted evolution of the excitation probability as a function of the delay within these conditions. Compared with Fig. 6(a), the general shape is more similar to the TDDFT one of Fig. 1(b) where the amplitude of oscillations decreases more by increasing the delay. We have checked it is due to going from one conduction state to ten. Summing the ten contributions break partially the coherence because of using different bandgaps. Also this configuration prevents from producing less excited electrons with two-pulse irradiation than with the independent sum of two single-pulse irradiation. With one conduction state, a delay can lead to a two-pulse maximum electric field amplitude smaller than single-pulse one due to interference-like effect (despite the photon energies are different, the broad spectrum due to the very finite pulse duration includes such an effect), leading to a lowered electron excitation. In case of ten conduction states with partial loss of resonance, summing various contributions remove the dependence on the interference-like effect. TDDFT calculations include an even more complex band structure so that this effect is enhanced, leading to observable oscillations only for the shortest delays (Fig. 1). Regarding the enhancement ratio in the production of excited electrons, it is 5.4 within these conditions, which significantly departs from the TDDFT prediction of 14.3. This discrepancy seems to be due to the significant difference in the excitated electron probability induced by single pulses ($P_1 = 2.5 \times 10^{-6}$ versus $P_2 = 1.5 \times 10^{-3}$). This result further confirms the influence of mixing photon energies with various combinations to bridge the bandgap. The latter process is the most significant when both color contributions are similar, leading to a similar contribution of each combination to the excitation probability. In case of strong imbalance between pure color excitation, such a cooperation is no longer possible, explaining the smaller enhancement (we have checked this behavior reproduces whatever the number of conduction states).

Since the previous considerations on the enhancement factor are based on pure multiphoton absorption, the last performed BVkP calculation addresses this perturbative regime by using the lowest intensities conditions of Fig. 1(a) in the TW/cm^2 range. To reproduce required conditions for a large enhancement for which $P_1 = P_2$, the laser intensity of the ω pulse is varied whereas the one of the 2ω pulse is the same as in Fig. 1(a). With the same material parameters as previously for Fig. 6(b) ($E_g = 9.05$ eV and the conduction band is described with ten states), we obtain $P_1 = P_2 = 1.4 \times 10^{-6}$ with $I_1 = 1.8 \times 10^{13}$ W/cm^2 and $I_2 = 10^{12}$ W/cm^2. The enhancement in the excited electron production is of the order of 35, which is again rather close to the TDDFT prediction of $\sim$30.

3. Analytical analysis of the enhancement in the free electron production based on the BVkP approach

Numerical results of the main text, predicted by both TDDFT and BVkP approaches, exhibit an enhancement of the laser produced conduction electron density when both pulses overlap. Based on analytical considerations with the BVkP approach, we show here this enhancement results from the opening of additional quantum ionization pathways due to combinations of both photon energies to bridge the bandgap. To demonstrate these additional possibilities, we show that the BVkP approach includes all this pathways by considering the energy conservation. Eq. (A2) is rewritten as

$$T_{cv}(\tau) = \int_0^\tau dt \exp\{iE_g t\} \sum_{n=0}^{\infty} \frac{i^{n-1}}{n!} A(t)^n E(t) \langle \phi_c | r^n | \phi_v \rangle, \tag{A3}$$

where the temporal integral $I_n = \int_0^\tau dt e^{iE_g t} A(t)^n E(t)$ ensures the energy conservation. Indeed, in the case of a single field, assuming the vector potential reads $A(t) = A_1 \exp(-i\omega t)$ for simplification purposes, $I_n \propto \int_0^\tau dt \exp(i(E_g - (n+1)\omega)t)$, which is the largest when $E_g - (n+1)\omega = 0$, i.e., when the simultaneous absorption of $n+1$ photons bridges the bandgap. The sum over n in Eq. (A3) then selects the most

probable ionization pathway corresponding to energy conservation. Note that there is in general a single ionization pathway. In case of two laser pulses with $A(t) = A_1 \exp(-i\omega_1 t) + A_2 \exp(-i\omega_2 t)$, the temporal integration reads:

$$I_n = i \int_0^\tau dt e^{iE_g t} (A_1 \exp(-i\omega_1 t) + A_2 \exp(-i\omega_2 t)) \times \sum_{k=0}^{n} C_n^k A_1^{n-k} A_2^k e^{-i(n-k)\omega_1 t} e^{-ik\omega_2 t} \quad \text{(A4)}$$

where C_n^k is the combinational number. Here there are two phases in the exponential functions, which make the integral the largest when they vanish, i.e., $E_g - (n-k+1)\omega_1 - k\omega_2 = 0$ and $E_g - (n-k)\omega_1 - (k+1)\omega_2 = 0$. Or, in the case of a given field and its first harmonics where $\omega_2 = 2\omega_1$, $E_g - (n+k+1)\omega_1 = 0$ and $E_g - (n+k+2)\omega_1 = 0$. Both sums over n and k leads to various combinations of both photon energies ensuring the energy conservation, thus increasing the number of ionization pathways and the transition amplitude. Therefore, the simultaneous irradiation with two pulses enhances the conduction electron production compared with two independent irradiations (where the pulse-to-pulse delay is such that pulses do not overlap). Note that considering fields written as a real function with a temporal envelope leads to more complicated calculations but with the same conclusion on electron production enhancement.

[1] X. Liu, D. Du, and G. Mourou, IEEE J. Quantum Electron. **33**, 1706 (1997).
[2] A.-C. Tien, S. Backus, H. Kapteyn, M. Murnane, and G. Mourou, Phys. Rev. Lett. **82**, 3883 (1999).
[3] M. D. Shirk and P. A. Molian, J. Laser Appl. **10**, 18 (1998).
[4] N. M. Bulgakova and V. P. Zhukov, *Continuum Models of Ultrashort Laser–Matter Interaction in Application to Wide-Bandgap Dielectrics* (Springer International Publishing, New York, 2014), pp. 101–124.
[5] G. Duchateau, B. Chimier, S. Coudert, E. Smetanina, L. Barilleau, N. Fedorov, H. Jouin, G. Geoffroy, P. Martin, and V. T. Tikhonchuk, Phys. Rev. B **102**, 024305 (2020).
[6] P. G. Hawkins, M. Y. Ivanov, and V. S. Yakovlev, Phys. Rev. A **91**, 013405 (2015).
[7] M. Wu, S. Ghimire, D. A. Reis, K. J. Schafer, and M. B. Gaarde, Phys. Rev. A **91**, 043839 (2015).
[8] N. S. Shcheblanov and T. E. Itina, Appl. Phys. A **110**, 579 (2013).
[9] L. Barilleau, G. Duchateau, B. Chimier, G. Geoffroy, and V. Tikhonchuk, J. Phys. D **49**, 485103 (2016).
[10] T. Apostolova and Y. Hahn, J. Appl. Phys. **88**, 1024 (2000).
[11] E. N. Glezer, M. Milosavljevic, L. Huang, R. J. Finlay, T.-H. Her, J. P. Callan, and E. Mazur, Opt. Lett. **21**, 2023 (1996).
[12] E. Gamaly, Phys. Rep. **508**, 91 (2011).
[13] A. Marcinkevičius, S. Juodkazis, M. Watanabe, M. Miwa, S. Matsuo, H. Misawa, and J. Nishii, Opt. Lett. **26**, 277 (2001).
[14] R. Gattass and E. Mazur, Nat. Photonics **2**, 219 (2008).
[15] J. Zhang, M. Gecevicius, M. Beresna, and P. G. Kazansky, Phys. Rev. Lett. **112**, 033901 (2014).
[16] M. Mero, B. R. Clapp, J. C. Jasapara, W. G. Rudolph, D. Ristau, K. Starke, J. Kruger, S. Martin, and W. Kautek, Opti. Eng. **44**, 051107 (2005).
[17] L. V. Keldysh, Zh. Eksp. Teor. Fiz. **47**, 1945 (1964) [Sov. Phys. JETP **20**, 1307 (1965)].
[18] A. Kaiser, B. Rethfeld, M. Vicanek, and G. Simon, Phys. Rev. B **61**, 11437 (2000).
[19] B. N. Yatsenko, H. Bachau, A. Belsky, J. Gaudin, G. Geoffroy, S. Guizard, P. Martin, G. Petite, A. Philippov, and A. N. Vasil'ev, Phys. Status Solidi C **2**, 240 (2005).
[20] H. Bachau, A. N. Belsky, P. Martin, A. N. Vasil'ev, and B. N. Yatsenko, Phys. Rev. B **74**, 235215 (2006).
[21] A. N. Vasil'ev, Y. Fang, and V. V. Mikhailin, Phys. Rev. B **60**, 5340 (1999).
[22] B. Rethfeld, Phys. Rev. Lett. **92**, 187401 (2004).
[23] J. R. Gulley and T. E. Lanier, in *Laser-Induced Damage in Optical Materials: 2015*, edited by G. J. Exarhos, V. E. Gruzdev, J. A. Menapace, D. Ristau, and M. Soileau, *International Society for Optics and Photonics* (SPIE, 2015), Vol. 9632, pp. 173–179.
[24] A. N. Pfeiffer, J. Phys. B: At., Mol. Opt. Phys. **53**, 164002 (2020).
[25] E. Smetanina, P. González de Alaiza Martínez, I. Thiele, B. Chimier, A. Bourgeade, and G. Duchateau, Phys. Rev. E **101**, 063206 (2020).
[26] O. Schubert, M. Hohenleutner, F. Langer, B. Urbanek, C. Lange, U. Huttner, D. Golde, T. Meier, M. Kira, S. W. Koch, and R. Huber, Nat. Photonics **8**, 119 (2014).
[27] S. Lagomarsino, S. Sciortino, B. Obreshkov, T. Apostolova, C. Corsi, M. Bellini, E. Berdermann, and C. J. Schmidt, Phys. Rev. B **93**, 085128 (2016).
[28] B. Obreshkov and T. Apostolova, Bulg. J. Phys. **42**, 305 (2015).
[29] E. Runge and E. K. U. Gross, Phys. Rev. Lett. **52**, 997 (1984).
[30] C. A. Ullrich, *Time-Dependent Density-Functional Theory: Concepts and Applications* (Oxford University Press, New York, 2012).
[31] T. Otobe, M. Yamagiwa, J.-I. Iwata, K. Yabana, T. Nakatsukasa, and G. F. Bertsch, Phys. Rev. B **77**, 165104 (2008).
[32] N. Tancogne-Dejean, O. D. Mücke, F. X. Kärtner, and A. Rubio, Phys. Rev. Lett. **118**, 087403 (2017).
[33] A. Yamada and K. Yabana, Eur. Phys. J. D **73**, 87 (2019).
[34] M. Noda, S. A. Sato, Y. Hirokawa, M. Uemoto, T. Takeuchi, S. Yamada, A. Yamada, Y. Shinohara, M. Yamaguchi, K. Iida *et al.*, Comput. Phys. Commun. **235**, 356 (2019).
[35] K. Krieger, J. K. Dewhurst, P. Elliott, S. Sharma, and E. K. U. Gross, J. Chem. Theory Comput. **11**, 4870 (2015).
[36] Y. Miyamoto and A. Rubio, J. Phys. Soc. Jpn. **87**, 041016 (2018).
[37] S. Y. Kruchinin, F. Krausz, and V. S. Yakovlev, Rev. Mod. Phys. **90**, 021002 (2018).
[38] J. Liao and J. R. Gulley, J. Opt. Soc. Am. B **31**, 2973 (2014).
[39] P. G. d. A. Martínez, E. Smetanina, I. Thiele, B. Chimier, and G. Duchateau, Phys. Rev. A **103**, 033107 (2021).

[40] S. Zoppel, J. Zehetner, and G. A. Reider, Appl. Surf. Sci. **253**, 7692 (2007).
[41] N. M. Bulgakova, V. P. Zhukov, J. Sldek, I. Mirza and A. V. Bulgakov, Dual Wavelength Laser Excitation of Bandgap Materials Challenges for Efficient Energy Coupling, *2020 Conference on Lasers and Electro-Optics (CLEO)* (OSA, 2020), pp. 1–2.
[42] F. Krausz and M. Ivanov, Rev. Mod. Phys. **81**, 163 (2009).
[43] M. Gedvilas, J. Mikšys, J. Berzinš, V. Stankevič, and G. Račiukaitis, Sci. Rep. **7**, 5218 (2017).
[44] X. Yu, Q. Bian, B. Zhao, Z. Chang, P. B. Corkum, and S. Lei, Appl. Phys. Lett. **102**, 101111 (2013).
[45] N. M. Bulgakova, V. P. Zhukov, A. R. Collins, D. Rostohar, T. J.-Y. Derrien, and T. Mocek, Appl. Surf. Sci. **336**, 364 (2015).
[46] A. Bourgeade and G. Duchateau, Phys. Rev. E **85**, 056403 (2012).
[47] G. Duchateau and A. Bourgeade, Phys. Rev. A **89**, 053837 (2014).
[48] T. Otobe, K. Yabana, and J.-I. Iwata, J. Phys.: Condens. Matter **21**, 064224 (2009).
[49] K.-M. Lee, C. Min Kim, S. A. Sato, T. Otobe, Y. Shinohara, K. Yabana, and T. Moon Jeong, J. Appl. Phys. **115**, 053519 (2014).
[50] S. A. Sato, K. Yabana, Y. Shinohara, T. Otobe, K.-M. Lee, and G. F. Bertsch, Phys. Rev. B **92**, 205413 (2015).
[51] G. F. Bertsch, J.-I. Iwata, A. Rubio, and K. Yabana, Phys. Rev. B **62**, 7998 (2000).
[52] K. Yabana and G. F. Bertsch, Phys. Rev. B **54**, 4484 (1996).
[53] S. A. Sato, M. Lucchini, M. Volkov, F. Schlaepfer, L. Gallmann, U. Keller, and A. Rubio, Phys. Rev. B **98**, 035202 (2018).
[54] S. A. Sato, Y. Taniguchi, Y. Shinohara, and K. Yabana, J. Chem. Phys. **143**, 224116 (2015).
[55] D. R. Lide, *CRC Handbook of Chemistry and Physics* (CRC Press, 2004), 79th edition.
[56] B. B. Karki and J. Crain, J. Geophys. Res. **103**, 12405 (1998).
[57] K. P. Driver, Proc. Natl. Acad. Sci. USA **107**, 9519 (2010).
[58] F. Tran and P. Blaha, Phys. Rev. Lett. **102**, 226401 (2009).
[59] K. Gaudfrin, J. Lopez, K. Mishchik, L. Gemini, R. Kling, and G. Duchateau, Opt. Express **28**, 15189 (2020).
[60] D. G. Arbó, C. Lemell, S. Nagele, N. Camus, L. Fechner, A. Krupp, T. Pfeifer, S. D. López, R. Moshammer, and J. Burgdörfer, Phys. Rev. A **92**, 023402 (2015).
[61] Y. P. Deng, X. H. Xie, H. Xiong, Y. X. Leng, C. F. Cheng, H. H. Lu, R. X. Li, and Z. Z. Xu, Opt. Express **13**, 3096 (2005).
[62] T. J.-Y. Derrien, N. Tancogne-Dejean, V. P. Zhukov, H. Appel, A. Rubio, and N. M. Bulgakova, Phys. Rev. B **104**, L241201 (2021).
[63] G. Duchateau, S. X. Hu, A. Pineau, A. Kar, B. Chimier, A. Casner, V. Tikhonchuk, V. N. Goncharov, P. B. Radha, and E. M. Campbell, Phys. Rev. E **100**, 033201 (2019).
[64] V. Nathan, A. H. Guenther, and S. S. Mitra, J. Opt. Soc. Am. B **2**, 294 (1985).
[65] G. Duchateau, E. Cormier, H. Bachau, and R. Gayet, Phys. Rev. A **63**, 053411 (2001).
[66] H. Jouin, M. Raynaud, G. Duchateau, G. Geoffroy, A. Sadou, and P. Martin, Phys. Rev. B **89**, 195136 (2014).
[67] W. V. Houston, Phys. Rev. **57**, 184 (1940).
[68] J. Callaway, *Quantum Theory of the Solid State* (Academic Press, New York, 1974).
[69] F. Schlaepfer, M. Lucchini, and S. A. Sato, M. Volkov, L. Kasmi, N. Hartmann, A. Rubio, L. Gallmann, and U. Keller, Nat. Phys. **14**, 560 (2018).